1-1-1992

Electrode Heating in a Wire-to-Plane Arc

Milind A. Jog
University of Pennsylvania

Ira M. Cohen
University of Pennsylvania

Portonovo S. Ayyaswamy
University of Pennsylvania, ayya@seas.upenn.edu

Electrode Heating in a Wire-to-Plane Arc

Abstract
A steady wire-to-plane electric discharge has been modeled in a prolate spheroidal coordinate system with the wire shape taken as a hyperboloid of revolution. A set of continuum conservation equations for the charged particle densities and temperatures together with Poisson's equation for the self-consistent electric potential describe the steady electric discharge process. These equations have been solved numerically to obtain ion and electron densities, temperature distribution, and electrode heat fluxes. Particle densities show the main body of the arc is quasineutral bounded by space charge sheaths at both electrodes. The temperature is greatest in a region around the discharge axis about one-third of the distance from the wire to the plane. Strong electric fields are concentrated in the electrode sheaths. The heat flux to the wire is sharply peaked near the tip but on the plane it decays slowly away from the discharge axis. The knowledge of heat transfer from the arc to the electrodes is useful in determining arc parameters that govern the ball formation process used in wire bonding of microelectronic semiconductor chips as well as welding processes.

Disciplines
Engineering | Mechanical Engineering

Comments
Suggested Citation:
Jog, Milind A., Ira M. Cohen and Portonovo S. Ayyaswamy. (1992) *Electrode heating in a wire-to-plane arc.* Physics of Fluids. Vol. 4(2).

Electrode heating in a wire-to-plane arc

M. A. Jog, I. M. Cohen, and P. S. Ayyaswamy
Department of Mechanical Engineering and Applied Mechanics, University of Pennsylvania, Philadelphia, Pennsylvania 19104-6315

(Received 11 March 1991; accepted 9 October 1991)

A steady wire-to-plane electric discharge has been modeled in a prolate spheroidal coordinate system with the wire shape taken as a hyperboloid of revolution. A set of continuum conservation equations for the charged particle densities and temperatures together with Poisson's equation for the self-consistent electric potential describe the steady electric discharge process. These equations have been solved numerically to obtain ion and electron densities, temperature distribution, and electrode heat fluxes. Particle densities show the main body of the arc is quasineutral bounded by space charge sheaths at both electrodes. The temperature is greatest in a region around the discharge axis about one-third of the distance from the wire to the plane. Strong electric fields are concentrated in the electrode sheaths. The heat flux to the wire is sharply peaked near the tip but on the plane it decays slowly away from the discharge axis. The knowledge of heat transfer from the arc to the electrodes is useful in determining arc parameters that govern the ball formation process used in wire bonding of microelectronic semiconductor chips as well as welding processes.

I. INTRODUCTION

In this paper, we consider a wire-to-plane steady arc discharge. The motions of ions and electrons in a continuum plasma, together with the self-consistent electric field with realistic ionization and recombination as well as a reasonable model for boundary conditions have all been examined. For simplicity in application of the boundary conditions, the wire is modeled as a hyperboloid of revolution in prolate spheroidal coordinates. We have obtained results for ion and electron densities, particle fluxes, temperature distribution, self-consistent electric field, and heat fluxes to both electrodes. Particle densities show the main body of the arc is quasineutral bounded by space charge sheaths at both electrodes. The temperature is greatest in a region around the discharge axis about one-third of the distance from the wire to the plane. Strong electric fields are concentrated in the electrode sheaths. The heat flux to the wire is sharply peaked near the tip but on the plane it decays slowly away from the discharge axis.

A wire-to-plane arc, such as that investigated here, is used to provide heat to a fine wire for the purpose of melting and forming a ball used in wire bonding of microelectronic semiconductor integrated circuit chips. Heretofore, arc parameters in such circumstances have been set empirically. Only very recently has a highly simplified model of this type of arc been analyzed by Vacek and Cohen.[1] The wire heat flux values obtained in the present study are consistent with our previous studies of simulation of wire melting and ball formation process. The time required to melt a portion of wire, about 15 diam long, was also found to be in agreement with the observations of ball formation from fine wires, thus lending credibility to our numerical investigation.

II. MATHEMATICAL FORMULATION

Once an electric arc is established, the transient changes in the arc parameters are small, and a steady-state analysis is adequate to determine the arc parameters and the heat transfer from the arc plasma to the electrodes. We consider an arc plasma consisting of three types of particles: electrons, ions, and neutrals. Good collision coupling exists between heavy particles and it can be assumed that ions and neutrals are at the same temperature. We focus our attention on arcs at atmospheric pressure. For these arcs it can be assumed that the difference between electron temperature and ion temperature is very small.[2] In the following analysis, ion, electron, and neutral temperatures are considered to be equal at a given location. The discharge is assumed to be axially symmetric. A set of continuum conservation equations for charged particle densities and temperatures together with Poisson's equation for the self-consistent electric potential adequately describe the electric discharge process.[3,4] The equations are

$$\nabla\cdot\boldsymbol{\Gamma}_e = P - R, \tag{1}$$

$$\nabla\cdot\boldsymbol{\Gamma}_i = P - R, \tag{2}$$

$$\nabla\cdot\mathbf{q}_e = -e\boldsymbol{\Gamma}_e\cdot\mathbf{E}, \tag{3}$$

$$\nabla\cdot\mathbf{q}_i = e\boldsymbol{\Gamma}_i\cdot\mathbf{E}, \tag{4}$$

$$\nabla\cdot\mathbf{E} = -(e/\epsilon_0)(N_e - N_i), \tag{5}$$

where the particle fluxes are given by

$$\boldsymbol{\Gamma}_e = -(\mu_e/e)\nabla(N_e kT_e) + \mu_e N_e \nabla V,$$
$$\boldsymbol{\Gamma}_i = -(\mu_i/e)\nabla(N_i kT_i) - \mu_i N_i \nabla V.$$

In the above, P and R are the production and recombination rates, respectively, and the heat fluxes are

$$\mathbf{q}_e = \tfrac{5}{2}kT_e\boldsymbol{\Gamma}_e - \chi_e \nabla T_e,$$
$$\mathbf{q}_i = \tfrac{5}{2}kT_i\boldsymbol{\Gamma}_i - \chi_i \nabla T_i,$$

with

$$\mathbf{E} = -\nabla V.$$

Here, N represents charged particle number density, T is the temperature, V is the electric potential, $\mathbf{E}$ is the electric field, μ are the mobilities, χ are the thermal conductivities, k is Boltzmann's constant, ϵ_0 is the permittivity of free space,

 0899-8221/92/020465-08$04.00

and e is the magnitude of electric charge on a single electron. The subscripts e and i are used for electrons and ions, respectively.

As the discharge develops from the transient breakdown phase to become self-sustaining, the charged particle densities increase many decades. The effect of space charge on the initial potential distribution consequently increases. However, for perfectly absorbing electrodes, these high charged particle densities drop steeply near the electrodes, forming sheath regions with high temperature and density gradients. Although the governing equations remain the same for the sheath and the main regions, the magnitudes of individual terms in Eqs. (1)–(5) are vastly different in different portions of the arc. Thus we may simplify the governing equations by scaling each term appropriately.

Let us first consider the central portion of the arc where the charged particle densities and temperatures are high. We scale V with applied voltage, gradients with gap length L, and nondimensionalize number densities with the number density, which will make the Debye length equal to the wire diameter, $N_R = kT_\infty \epsilon_0/e^2d^2$. Here d is the wire diameter. When the number densities are 1 or smaller, the left-hand side of Eq. (5) dominates over the right-hand side. As the number densities grow to 10^4, the left-hand side becomes two decades smaller than the right-hand side, and the zeroth-order solution in this case is

$$N_e = N_i = N.$$

Substituting this solution, using the assumption $T_e = T_i = T_n = T$, multiplying Eq. (1) by μ_i and Eq. (2) by μ_e, and adding and subtracting these two equations, we obtain, respectively,

$$\nabla\cdot\nabla(NT) = -[(\mu_i + \mu_e)/2\mu_i\mu_e](e/k)(P - R), \quad (6)$$

$$\nabla\cdot(N\nabla V) = [(\mu_i - \mu_e)/2\mu_i\mu_e](P - R). \quad (7)$$

Similarly, scaling T by 1 eV, we see that the thermal conduction terms in Eqs. (3) and (4) are orders of magnitude smaller than the remaining terms. With the neglect of these terms, multiplying Eq. (3) by μ_i and Eq. (4) by μ_e and adding the two equations, we obtain

$$\nabla\cdot[T\nabla(NT)] = -\tfrac{2}{5}(e^2/k^2)N\nabla V\cdot\nabla V. \quad (8)$$

Let us now look at the ionization mechanisms. Electron impact ionization, thermal ionization, and three body recombination govern the production and recombination of ions and electrons in the arc discharge. Electron impact ionization is given by

$$P = \alpha_i\mu_e E N_e,$$

where the Townsend's first ionization coefficient α_i depends on the electric field according to the relation

$$\alpha_i = A_i p \exp(-B_i p/E).$$

Here, A_i and B_i are constants that depend upon the type of gas under consideration. Here α_i is practically zero for values of the electric field below a threshold value. As the electric field in the main region of the arc is expected to be below this threshold, ionization by electron impact should be negligible in the main region of the discharge. However, this ionization mechanism is important in the sheath regions. Net production by thermal ionization and three body recombination is given by the Saha equation as[5]

$$P - R = \gamma N_e \left[\frac{2g_i N_n}{g_n}\left(\frac{2\pi m_e kT_e}{h^2}\right)^{3/2} \times \exp\left(-\frac{eV_i}{kT_e}\right) - N_e N_i\right], \quad (9)$$

where γ depends on electron temperature as[6]

$$\gamma = 1.09\times 10^{-20} T_e^{-9/2} \text{ m}^6/\text{sec}.$$

Here, N_n is the neutral number density, g_i is the statistical weight of ions, g_n is the statistical weight of the ground state of the neutral particles, m_e is the mass of an electron, V_i is the ionization potential of the ground state, and h is Planck's constant.

The first term on the right-hand side of Eq. (9) has an exponential dependence on temperature. The right-hand side shows a balance between two very large numbers compared to the left-hand side. A small change in temperature results in a large difference in the two terms on the right-hand side compared to the left-hand side. Therefore, for the zeroth-order solution, the two terms on the right-hand side must be equal. With this simplification, the resulting governing equations for the main portion of the discharge are

$$\nabla\cdot(N\nabla V) = [(\mu_e - \mu_i)/(\mu_e + \mu_i)]\nabla\cdot\nabla(NT), \quad (10)$$

$$\nabla\cdot[T\nabla(NT)] = -\tfrac{2}{5}N\nabla V\cdot\nabla V, \quad (11)$$

$$N^2 = \frac{2g_i N_n}{g_n}\left(\frac{2\pi m_e eT}{h^2}\right)^{3/2}\exp\left(-\frac{V_i}{T}\right). \quad (12)$$

Here T is expressed in eV.

Boundary conditions. Several different boundary conditions for the particle densities and temperatures at the electrodes have been employed in past studies. An assumption of perfectly absorbing electrode surfaces would lead to zero particle density at the electrodes.[7] Chung[8] derived two sets of boundary conditions with and without emission at the surface. Graves and Jensen[9] have noted that the zero particle density at the electrodes may lead to considerable numerical difficulties. They have considered ion flux at the electrodes due only to drift. This leads to a nonzero ion density at the electrodes and avoids the very thin diffusion layers near the surfaces. This simplification reduces numerical difficulties without affecting the solution significantly. The electron flux at the cathode has been related to the incident ion flux through an emission coefficient.[8,10] In view of our interest in the wire bonding process, we are particularly interested in discharges with gold, aluminum, or copper as electrode materials. With these materials, a zero particle density seems to be an appropriate boundary condition due to small electron emission. However, to avoid the singular behavior that the zero density condition may lead to, we assign a nonzero but very small particle density to the electrodes. Numerical experimentation showed that the results do not change significantly if the assigned particle density value at the electrodes is nonzero and very small. Changing

the value by a factor of 5 affected the solutions by less than 1%. The total current is specified at each electrode surface. The surface temperature is specified as the melting temperature of the electrodes, a suitable condition for the discharges used for ball formation in wire bonding of microelectronic interconnections. Far away from the discharge axis the particle densities and the temperature are specified as their ambient values and the potential gradient is considered to become zero. The following sets are the appropriate boundary conditions: At the electrodes,

$$v = v_w, \quad N_e = N_i = N_0, \quad T_e = T_i = T_w, \quad I = I_w,$$
$$v = \pi/2, \quad N_e = N_i = N_0, \quad T_e = T_i = T_w, \quad I = I_w;$$

with the symmetry condition on the discharge axis,

$$u = 0, \quad \frac{\partial}{\partial u} = 0;$$

and, away from the discharge axis,

$$u \to \infty, \quad \frac{\partial V}{\partial u} \to 0, \quad N_e, N_i \to N_0, \quad \frac{\partial T}{\partial u} \to 0.$$

III. SOLUTION TECHNIQUE

The discharge is modeled in a prolate spheroidal coordinate system that provides a fine computational grid near the wire tip.[11] Figure 1 shows the schematic of the coordinate system. The wire shape is taken as a hyperboloid of revolution. The prolate spheroidal coordinates (u, v, ϕ) are related to the Cartesian coordinates as

$$x = a \sinh u \sin v \cos \phi,$$
$$y = a \sinh u \sin v \sin \phi, \tag{13}$$
$$z = a \cosh u \cos v,$$

where a is the semifocal distance. The wire corresponds to $v = v_w$, whereas the planar electrode is given by $v = \pi/2$. The wire diameter, taken as twice the tip radius, is $d = 2L \tan^2 v_w$. The gap length is related to the semifocal distance as $L = a \cos^2 v_w$.

The governing equations [Eqs. (10)–(12)] for the main portion of the discharge are solved using an underrelaxation technique for the entire domain. These equations are valid until the assumption of quasineutrality is violated. The assumption of quasineutrality can be invoked for densities greater than about 10^3. In our computational scheme, we choose points near the electrode where the density is 10^3, and then Eqs. (1)–(3) and (5) are solved proceeding toward the electrodes. The heavy particle temperature in the sheath region is considered to have a linear variation. Although the boundary condition on the charged particle flux equation is that of specified current, in the actual computational scheme voltages at the electrodes are specified and are iteratively changed in each run so as to get the required current at the electrode. The equations for the quasineutral portion of the arc are solved first and subsequently the equations for the sheath region are solved. The solution algorithm involves specifying initial guess values for the arc parameters. The governing equations are iterated upon to improve these initial values until the changes in all variables are below a specified convergence limit (relative error of 0.1%). Because of the highly nonlinear nature of the equations and a strong interdependence among variables, an underrelaxation coefficient of 0.1 is used to obtain convergence. A typical run on the PSC CRAY Y/MP took about 15 min for the main region and about 5 min for sheath solutions. Several iterations were needed to obtain the desired current value.

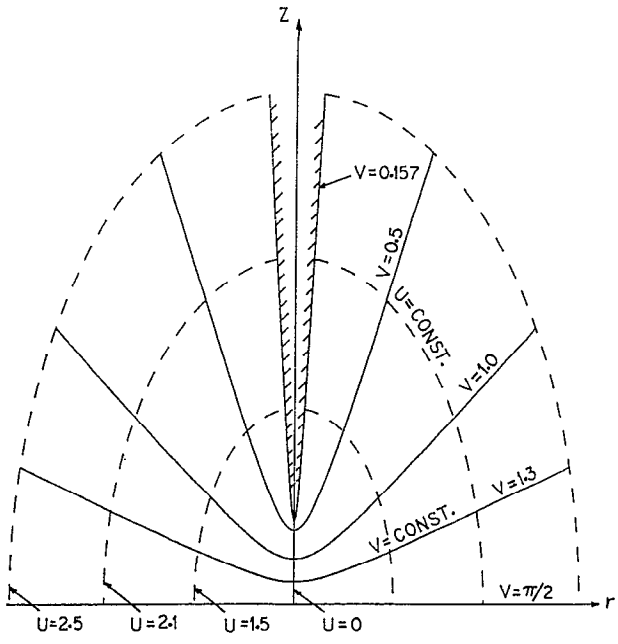

FIG. 1. Coordinate system.

IV. ELECTRODE HEAT TRANSFER

Apart from the particle density variations and temperature variations, our interest lies in determining the heat transfer to the electrodes. Owing to a lack of precise models and data, correlations with Gaussian variation or step function variation are usually employed for the heat flux from the arc to a planar electrode.[12,13] These correlations are inappropriate for the wire geometry. A number of surface phenomena contribute to the heat transport to the electrodes.[14–21] At the cathode the following effects are important.

(a) Energy is transferred to the cathode by recombination of the incoming ions with electrons that must be freed from the electrode surface. This requires energy equivalent to the work function for the electrode material. Therefore the total energy transferred to the cathode q_n is given by

$$q = a_n e \Gamma_{i,n} (V_i - \phi),$$

where a_n is the accommodation coefficient, which accounts for the fact that not all of the energy of neutralization is given to the cathode. Part of this energy is transformed into kinetic energy of the reflected particles. Here $\Gamma_{i,n}$ is the normal component of the ion density flux at the cathode.

(b) Ions also deposit their thermal energy q_c to the cathode by conduction. The thermal energy is given by

$$q = -\chi_i \nabla T_i.$$

Similarly, at the anode the following effects are important.

(1) The incoming electrons release energy equivalent to their work function to the anode given by

$$q = a_e e \Gamma_{e,n} \phi,$$

where a_e is the accommodation coefficient and $\Gamma_{e,n}$ is the normal component of the electron density flux at the anode.

(2) The conduction heat transfer at the anode surface is given by

$$q = -\chi_e \nabla T_e.$$

We note that the other modes of energy transport, viz., radiation loss from the electrode surfaces, and energy loss associated with metal evaporation or metal ejection would be small compared to the effects considered above.

V. RESULTS AND DISCUSSION

The calculations have been made for a total current of 0.1 A with the wire "diameter" d taken as 25 μm with positive as well as negative wire polarity. This results in the potential drop of about 140 V in the arc discharge. These parameters are typical of the ball formation discharge in the wire bonding process for microelectronic interconnections. The various other parameters used are $v_w = 0.157$, $d = 25 \times 10^{-6}$ m, $L = 5 \times 10^{-4}$ m, $N_0 = 6 \times 10^{8}$ m^{-3}, $N_n = 1.47 \times 10^{25}$ m^{-3}, $N_R = 2.36 \times 10^{16}$ m^{-3}, $p = 1.01 \times 10^{5}$ Pa, $\mu_e = 0.065\,79$ m^2/V sec, $\mu_i = 4.3856 \times 10^{-4}$ m^2/V sec, $T_\infty = 500$ K, $a_e = 0.9$, and $a_n = 0.25$. The discharge medium is air.

We first discuss results for positive wire polarity. Figure 2 shows the variation of the charged particle densities along the discharge axis. Near the cathode, the current is due mainly to ion drift, and the ion densities are much higher than the electron densities. On the other hand, near the anode, the total current is due mainly to electron drift. The ion densities fall very rapidly toward the anode whereas the electron densities decrease very slowly there. This shows that in the case of electrons, the drift mechanism dominates over the diffusion effect near the anode. The same is true of ions near the cathode. The ion densities are considerably higher than the electron densities near the cathode. The gradient of ion density becomes very small near the rod. This shows that the zero ion density gradient boundary condition used by Graves and Jensen[12] may be useful in reducing the computational difficulties without affecting the solution significantly. The electron densities are considerably higher than the ion densities. As the arc approaches the planar anode, the

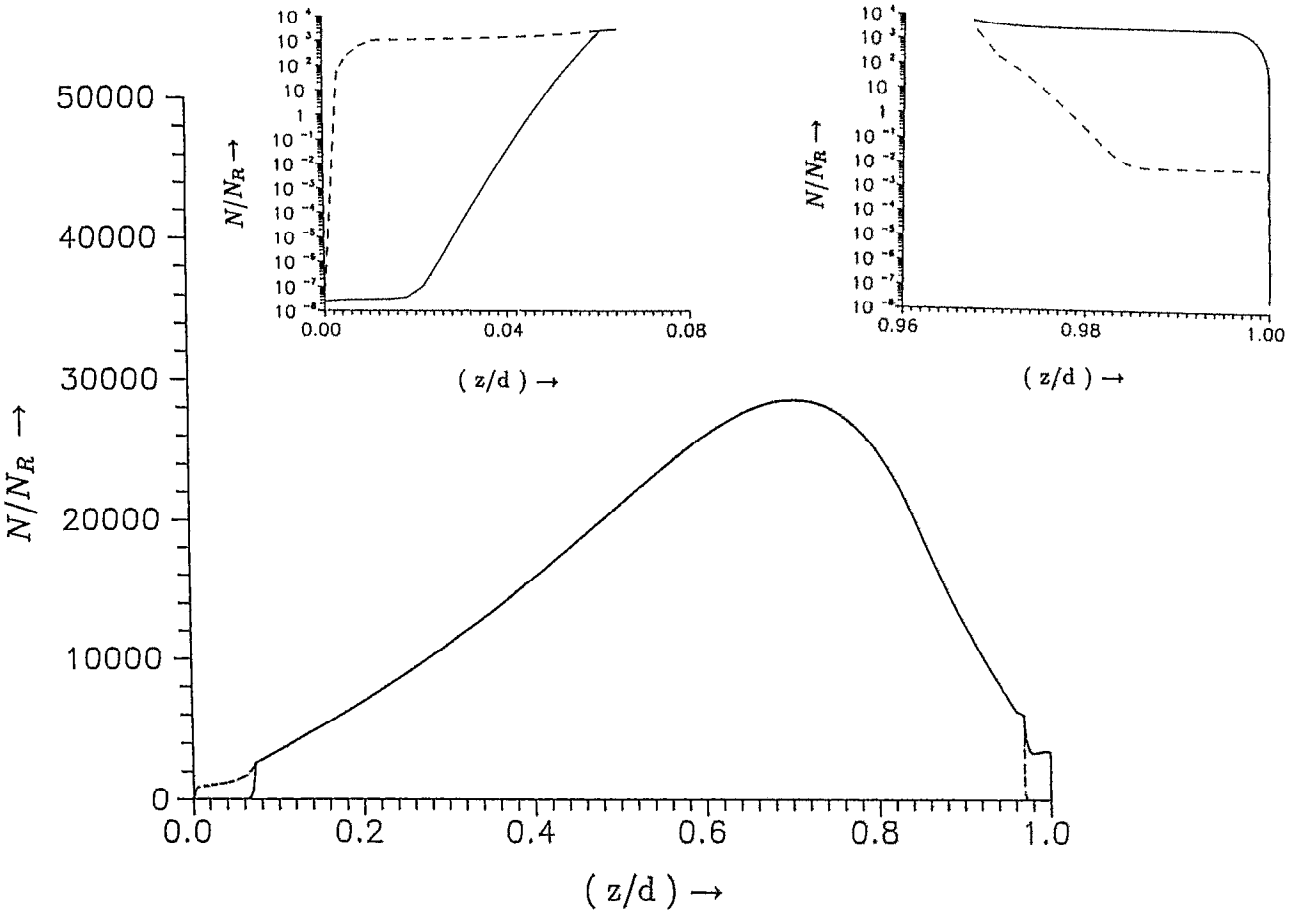

FIG. 2. Variation of charged particle densities along the discharge axis (positive wire). Legend: solid lines, electron number density; dotted lines, ion number density.

radial nonuniformities in the electric potential become very small compared to the level of nonuniformities in regions near the wire. The charged particle densities in the electrode sheath are small and the right-hand side of Poisson's equation that governs the electric field becomes small. Poisson's equation behaves like Laplace's equation resulting in an approximately linear increase in the electric potential very near the anode. Also, the charged particle production in the anode sheath region is low keeping the current nearly constant. This results in an almost constant electron number density near the anode. Figure 3 shows the potential variation along the discharge axis. Most of the voltage drop occurs near the electrodes. The variation in electric potential in the central portion of the discharge is less than one-tenth the total potential drop. Two effects play important roles in determining the cathode and the anode voltage drops. The voltage drop near the cathode is higher than that near the anode as the ion mobility is smaller than the electron mobility. The arc shape near the wire electrode is significantly different than that near the planar electrode. Hence, with negative wire polarity the cathode drop is greater than that with positive wire polarity.

Figure 4 shows isotherms in the arc. The maximum temperature occurs on the discharge axis and is at a point located about one-third the gap length from the wire tip. This point also corresponds to the location with maximum charged particle density. From the location of the maximum temperature, the temperature values drop away toward the wire and the planar electrode. The temperatures are also higher near the discharge axis than farther away from it.

Figure 5 shows the heat flux variation along the wire surface. With positive wire, the maximum heat flux occurs at the wire tip and decreases along the wire surface. The heat flux becomes less than one-tenth of its maximum value within four wire diameters. The heat flux variation along the planar electrode surface is shown in Fig. 6. The heat flux decreases more gradually with distance from the discharge axis. The maximum heat flux at the planar electrode is significantly less than that at the wire. The heat flux to the wire is sufficient to melt a length of about 15 diameters in a period of 1.5 msec, consistent with observations of ball formation

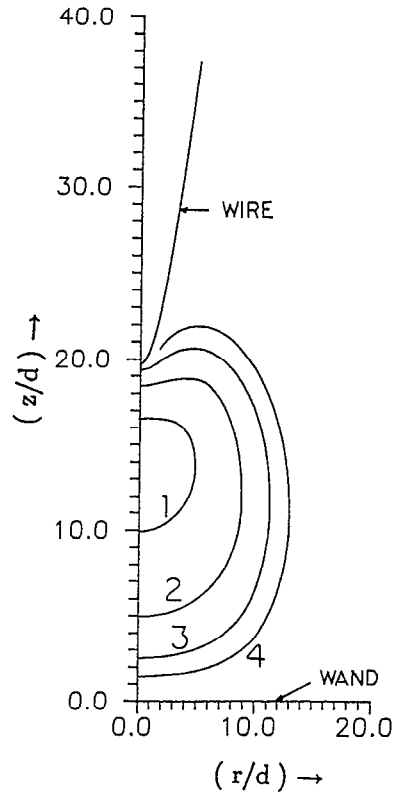

FIG. 4. Isotherms in the arc. Legend: (1) 6700 K, (2) 6300 K, (3) 6000 K, and (4) 5500 K.

from fine wires. The heat flux values are in close agreement with our previous studies[22] of modeling of wire melting and ball formation processes.

Figure 7 shows the axial variation of the charged particle densities with negative wire polarity. The ion densities fall very rapidly near the planar electrode and the electron densities fall rapidly near the wire. Although the qualitative

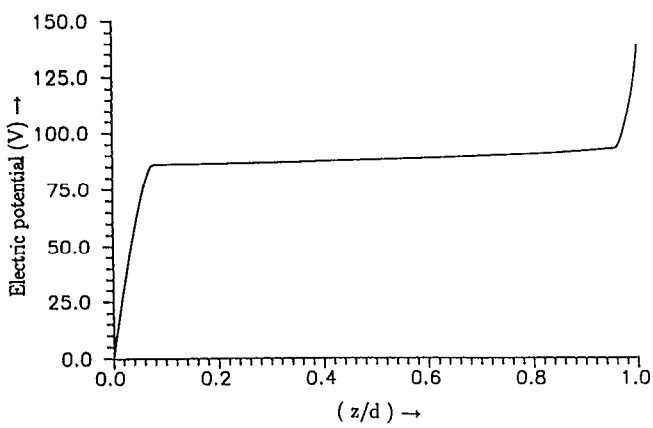

FIG. 3. Potential distribution along the discharge axis (positive wire).

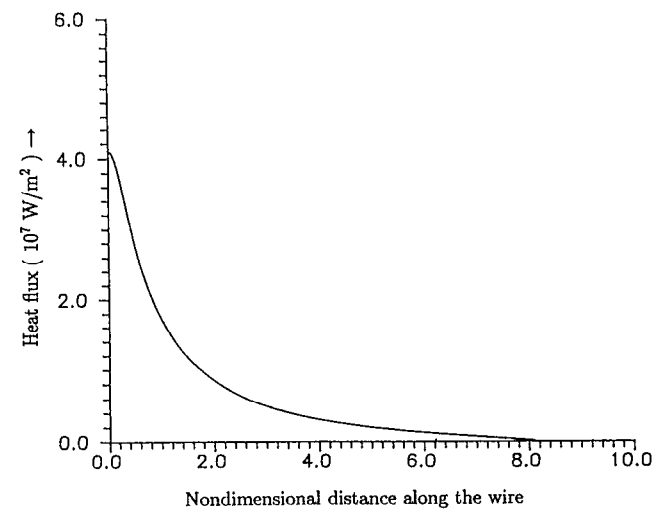

FIG. 5. Heat flux along the wire (positive wire).

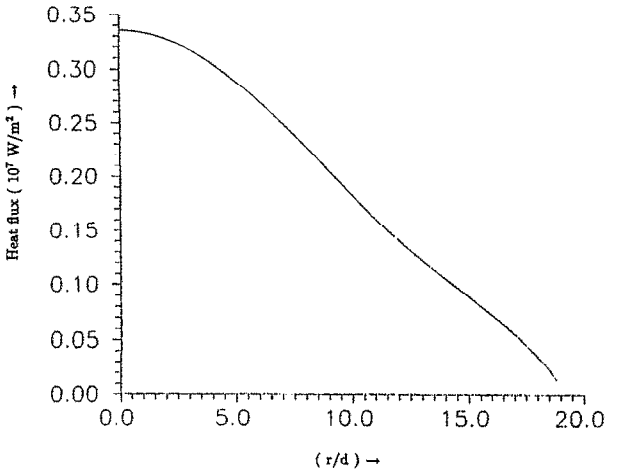

FIG. 6. Heat flux at planar electrode (positive wire).

nature of the axial variation of the charged particle densities with positive wire is similar to that with negative wire polarity, the axial potential variation differs significantly. Figure 8 shows the potential variation along the discharge axis. Most of the voltage drop occurs near the wire. The electron mobility is greater than the ion mobility. This results in a lower voltage drop near the planar electrode.

Figure 9 shows the variation of heat flux along the wire surface. The maximum heat flux does not occur on the discharge axis but slightly away from it. The heat flux decreases gradually along the wire surface resulting in significant heat transport to the wire from the sides. Our previous experiments[22] have shown that wire heating is mainly from the bottom surface in case of positive wire while with negative wire, heating is mainly from the sides. This result can be explained as follows. Near the rod the equipotential lines approximately coincide with $v = \text{const}$ lines. This variation in electric potential results in an axial flow of electrons from the discharge axis as the electrons move from the cathode toward the anode. The electron density increases slightly away from the discharge axis. As the production rate of charged particles is proportional to the electron density, ion density also increases slightly away from the discharge axis. The ion mobility is lower than the electron mobility and the axial flow of ions toward the discharge axis is small. This gives maximum ion current at a location slightly away from the discharge axis and hence the maximum heat flux occurs there. Figure 10 shows the heat flux variation along the planar electrode surface. The maximum heat flux occurs on the discharge axis and decreases with distance away from the discharge axis. For both polarities the heat flux to the anode

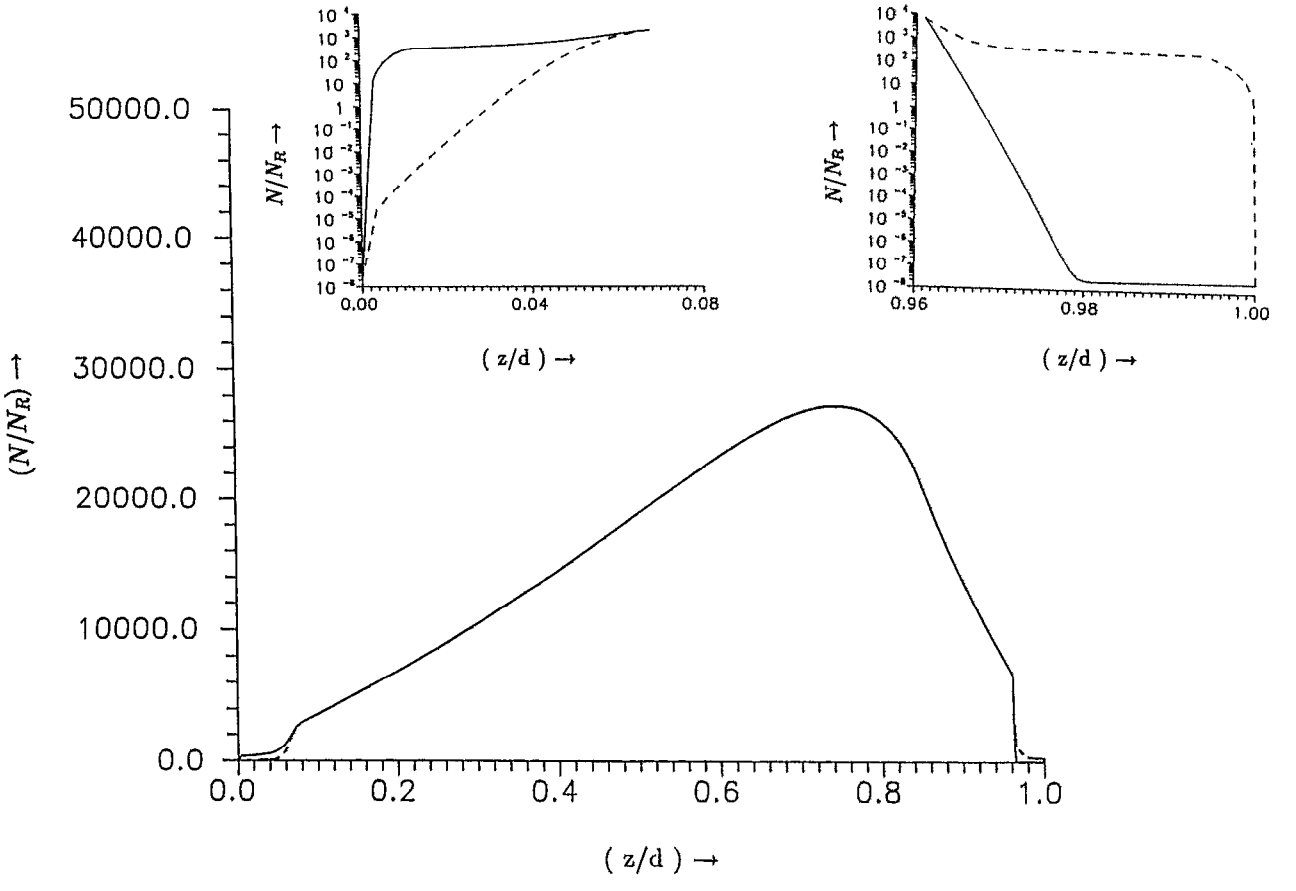

FIG. 7. Variation of charged particle densities along the discharge axis (negative wire). Legend: solid lines, electron number density; dotted lines, ion number density.

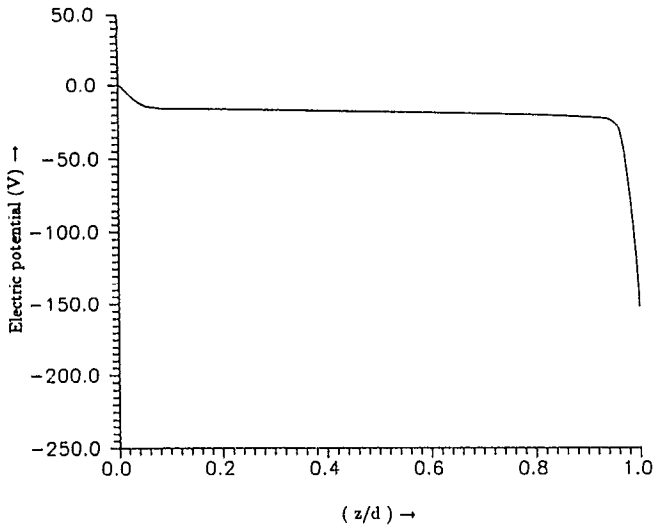

FIG. 8. Potential distribution along the discharge axis (negative wire).

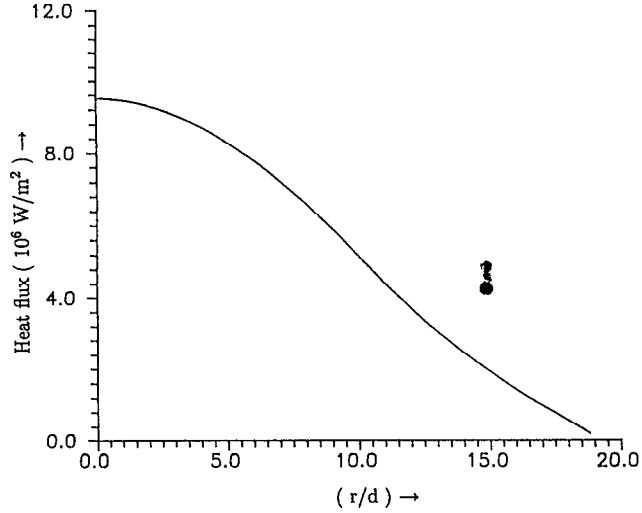

FIG. 10. Heat flux at planar electrode (negative wire).

is greater by more than an order of magnitude than the heat flux to the cathode primarily due to the greater electron mobility.

A rod-to-plane geometry is typically used in the industrial arc welding process. Previous studies[12,13] of melting, solidification, and flows in weld pools have used empirical heat flux distributions. The model presented here can be used to accurately determine the heat transfer from the arc to the workpiece and to the electrode.

VI. CONCLUSIONS

We have presented a two region model for a wire-to-plane steady electric discharge. The continuum conservation equations are solved to model the quasineutral and the electrode sheath regions in a prolate coordinate system. Charged particle densities, temperature, and electric potential variations are obtained for positive as well as negative wire polarity. From this study we can draw the following conclusions.

(1) When a wire is the anode, the maximum heat flux occurs at the wire tip and drops sharply away from the discharge axis. When a wire is the cathode, the maximum heat flux does not occur on the discharge axis and there is significant heating from the sides.

(2) Most of the potential drop occurs near the electrodes. The cathode drop is higher than the anode drop, and only about one-tenth of the total voltage drop occurs in the main region of the discharge.

(3) The maximum temperature occurs on the discharge axis and is at a point located about one-third the gap length from the wire tip. The high-temperature region spreads about ten wire diameters on the plane and about four wire diameters near the wire.

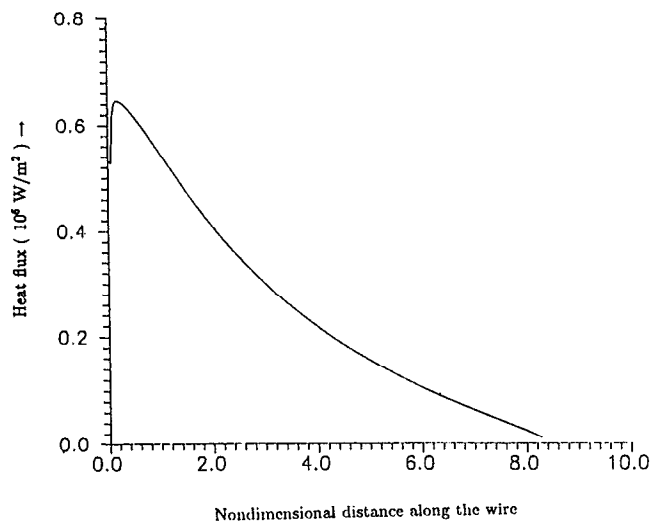

FIG. 9. Heat flux along the wire (negative wire).

ACKNOWLEDGMENTS

Computations were performed on PSC's CRAY Y/MP.

This work was supported by the National Science Foundation under Grants No. DMC 8709537 and No. DDM 9000573. Support for numerical computations was provided by the Pittsburgh Supercomputing Center under Grants No. DMC 0000000/8513128 and No. DMC 890001P.

[1] D. J. Vacek and I. M. Cohen, J. Appl. Phys. **65**, 1005 (1989).
[2] E. Pfender, in *Gaseous Electronics, Vol. 1—Electric Discharges*, edited by M. N. Hirsh and H. J. Oksam (Academic, New York, 1978), p. 291.
[3] W. P. Allis, in *Handbuch der Physik, XXI* (Springer-Verlag, Berlin, 1956), p. 383.
[4] D. R. Wilkins and E. P. Gyftopoulos, J. Appl. Phys. **37**, 3533 (1966).
[5] M. Mitchner and C. H. Kruger, *Partially Ionized Gases* (Wiley, New York, 1973), p. 78.
[6] E. Hinnov and J. G. Hirshberg, Phys. Rev. **125**, 795 (1962).
[7] I. M. Cohen, Phys. Fluids **8**, 2097 (1965).

[8] P. M. Chung, Phys. Fluids **12**, 1623 (1969).
[9] D. B. Graves and K. F. Jensen, IEEE Trans. Plasma Sci. **PS-14**, 78 (1986).
[10] P. Bayle, J. Vacquire, and M. Bayle, Phys. Rev. A **34**, 360 (1986).
[11] K. Ramakrishna, Ph.D. dissertation, University of Pennsylvania, 1989.
[12] J. G. Andrews and D. R. Atthey, Int. J. Heat Mass Transfer **22**, 1533 (1979).
[13] S. S. Glickstein and E. Friedman, Welding J. **63**, 38 (1984).
[14] J. D. Cobine and E. E. Burger, J. Appl. Phys. **26**, 895 (1955).
[15] J. D. Cobine, *Gaseous Conductors* (Dover, New York, 1958).
[16] G. Ecker, in *Ergebnisse der Exakten Naturwissenschaften* (Springer-Verlag, Berlin, 1961), p. 1.
[17] J. A. Augis, F. J. Gibson, and E. W. Gray, Int. J. Electron. **30**, 315 (1971).
[18] G. Ecker, in *Electrical Breakdown and Discharges in Gases*, edited by E. E. Kunhardt and L. H. Luessen (Plenum, New York, 1981), p. 167.
[19] N. Sanders, K. Etemadi, K. C. Hsu, and E. Pfender, J. Appl. Phys. **53**, 4136 (1982).
[20] K. C. Hsu and E. Pfender, J. Appl. Phys. **54**, 3818 (1983).
[21] N. A. Sanders and E. Pfender, J. Appl. Phys. **55**, 714 (1984).
[22] L. J. Huang, M. A. Jog, I. M. Cohen, and P. S. Ayyaswamy, Trans. ASME J. Electron. Pkg. **113**, 33 (1991).